Optica Applicata, Vol. XXXVIII, No. 4, 2008

Pure rotational Raman lidar with fiber Bragg grating for temperature profiling of the atmospheric boundary layer

JIANDONG MAO[1, 2], LIAOLIN HU[1], DENGXIN HUA[1, *], FEI GAO[1], MIN WU[1]

[1]School of Mechanical and Precision Instrument Engineering, Xi'an University of Technology, No. 5 South Jinhua Road, Xi'an 710048, China

[2]Department of Electronic and Information Engineering, The Second Northwest University for Nationalities, North Wenchang Road, Yinchuan, 750021, China

[*]Corresponding author: dengxinhua@xaut.edu.cn

A new pure rotational Raman lidar (PRRL) system at a wavelength of 532.25 nm has been designed for profiling the atmospheric temperature of the planetary boundary layer. A newly compact spectroscope structured with three fiber Bragg gratings (FBG) is designed to separate two pure rotational Raman signals for atmospheric temperature retrieval, and to simultaneously block the Mie- and Rayleigh-scattering signals with a rejection rate of 10^7. A numerical simulation shows that the PRRL is capable of profiling the atmospheric temperature and a statistical temperature error less than 1 K is achieved up to a height of 2.0 km and 2.2 km for daytime and nighttime measurement, respectively.

Keywords: pure rotational Raman lidar, fiber Bragg grating, temperature profiling.

1. Introduction

Temperature is one of important basic atmosphere parameters, which characterizes the state of the atmosphere and crucially affects the existence and life environment of human. Therefore, measurement of temperature profiles is of considerable importance for studies in the atmospheric science and accurate weather forecasting, particularly for research on urban climate, including heat-island phenomena, relative humidity retrievals, transport characteristic of aerosol and so on [1, 2].

Lidar has been considered to be one of the recently effective techniques and played an important role in remote sensing of atmosphere parameters with real-time and high spatial resolution. Raman lidar, as a powerful remote sensing technique of atmospheric temperature, has been studied for several decades. Using of the temperature dependence of the intensity of the pure rotational Raman spectral (PRRS) lines of atmospheric

N_2 and O_2 molecules was proposed firstly by Cooney for temperature profiling [3], and many groups have already reported the performance of PRRL and measurement results of temperature of the atmospheric boundary layer [4–10].

However, because Raman scattering cross section is 3–4 orders of magnitude smaller than Mie and Rayleigh', separating the weak Raman scattering signals from the intense background noise, including Mie- and Rayleigh-scattering signals and solar radiation light in the case of daytime, is the key technique that ensures the feasibility of high accurate temperature profiling in PRRL. Up to now, for separating the useful PRR signal effectively, the PRRL system employs usually high laser energy, large-diameter telescope, and uses especially complex spectroscope, such as interference filters, single grating monochromator in combination with an atomic resonance absorption filter or a double grating monochromator, *etc*. in practice. As a serious demerit, the complicated spectroscope may lead to the low efficiency and low reliability of lidar system and hence influences adversely the development of the PRRL for practical use.

Recently, the fiber Bragg grating (FBG) technique using single mode fiber has made progress rapidly and is widely applied in fiber communication and fiber sensor field because of its many useful features, such as, strict wavelength selection, narrow bandwidth, high spectral resolution, high out-of-band rejection rates, high stability, compactness, low mass and all-fiber connection, *etc*. Therefore, as a new spectroscopic filter, its potential for lidar application is noticeable. In practice, I. Stenholm and R. DeYoung of the NASA Langley Research Center have developed a space-based water vapor differential absorption lidar system based on spectroscopic technique of the FBG [11].

The main propose of this paper is to describe a concept design of new PRRL, based on filter characteristic of FBG and a numerical calculation for supporting the concept design.

2. Configuration of PRRL system using FBG

Figure 1 shows a block diagram of the PRRL system based on the FBG technique. A narrowband, injection-seeded, frequency doubled, pulsed Nd:YAG laser with a single longitudinal mode provides a required wavelength of 532.25 nm with an energy of 300 mJ at a pulse repetition of 20 Hz. The laser output is collimated by a 10× beam expander and transmitted into the atmosphere vertically with a divergence angle θ of 0.05 mrad. A 50-cm-diameter Cassegrainian telescope collects the atmospheric backscattered light and couples it into a standard single mode fiber (SMF) that sets the field of view of the receiving telescope at 0.01 mrad, and the SMF is connected with port 0 of spectroscope system directly.

The spectroscope system consists of three FBGs and corresponding optical circulators. The FBG reflects the light signal whose wavelength equals the Bragg wavelength and lets other wavelength light signal pass through. The Bragg wavelength

of three FBGs, FBG 1–FBG 3, is selected at λ_0 = 532.25 nm, λ_1 = 530.6 nm and λ_2 = 528.8 nm, respectively.

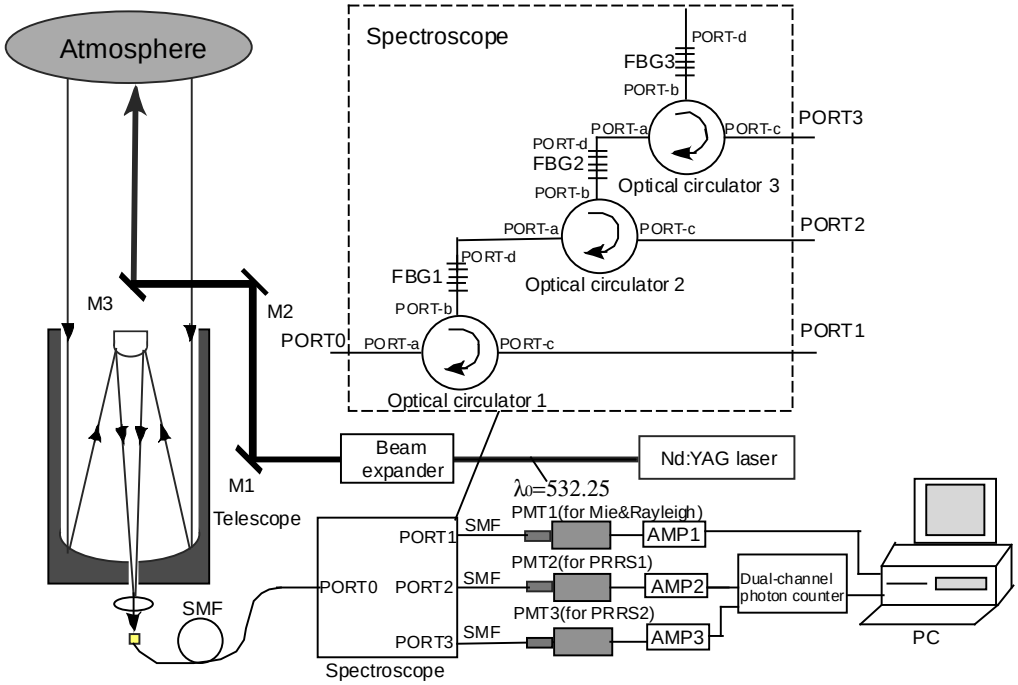

Fig. 1. Schematic of the PRRL system using the FBG (FBG – fiber Bragg grating, SMF – single-mode fiber, M1, M2, M3 – mirror, PMT – photomultiplier tube).

The lidar return light signal passing through port 0 is coupled into port-a of optical circulator 1 where light travels from port-a to port-b, then coupled into FBG 1 which reflects the major portion elastic signal, including Mie- and Rayleigh-scattering signals centered at λ_0, and lets other wavelength light transmit nearly entirely. The reflected elastic signal enters the optical circulator 1 again at port-b, leaves at port-c (PORT 1), is coupled into a SMF and then detected with a photomultiplier tube 1 (PMT1).

The other light which wavelength is not centered at λ_0 passes through the FBG1 and is directed into port-a of optical circulator 2, then is coupled into FBG2. The FBG 2 reflects the major portion low-quantum-number PRR signal located at central wavelength λ_1 and lets other wavelength light pass through. The reflected PRR signal returns to the optical circulator 2 again, and exits at port-c (PORT 2), then detected with a photomultiplier tube 2 (PMT2).

Similarly, the FBG3 and optical circulator 3 reflect the high-quantum-number PRR signal located at central wavelength λ_2, let the reflected PRR signal pass through the port 3, and then are detected with PMT3.

As a result, the elastic signal can be blocked effectively by not less than two FBGs and the two PRRSs are separated spatially from the lidar return.

The PMT outputs of two PRRSs channel are amplified by high-speed/low noise preamplifier before being sent to a dual-channel photon counter. The sampling rate of data acquisition is 300 ns, which corresponds to a range resolution of 45 m.

Generally, the multi-mode fiber is usually employed in practical lidar system. However, the FBG is mainly made from single mode fiber in practice; therefore, the single mode fiber is employed for our goal in this paper. Although the single mode fiber leads to decrease the receiving efficiency of lidar system, the low receiving efficiency is not an intrinsic problem and it can be improved by optimizing the lidar performance in practice.

3. Principle of temperature measurement

For avoiding the effect of atmospheric fluorescence generated from laser excitation and improving the temperature detection sensitivity of PRRL, the anti-Stokes branch is selected. Figure 2 shows an intensity distribution of anti-stokes PRRS of N_2 with a 532.25 nm laser excitation on atmospheric temperature of 200 K and 300 K and filter reflectivity of the FBG2 and FBG3. The central wavelength of the two FBGs for filtering the PRRSs is located at 530.6 nm and 528.8 nm, respectively, corresponding to the initial rotational-angular-momentum quantum number J of 6 and 14.

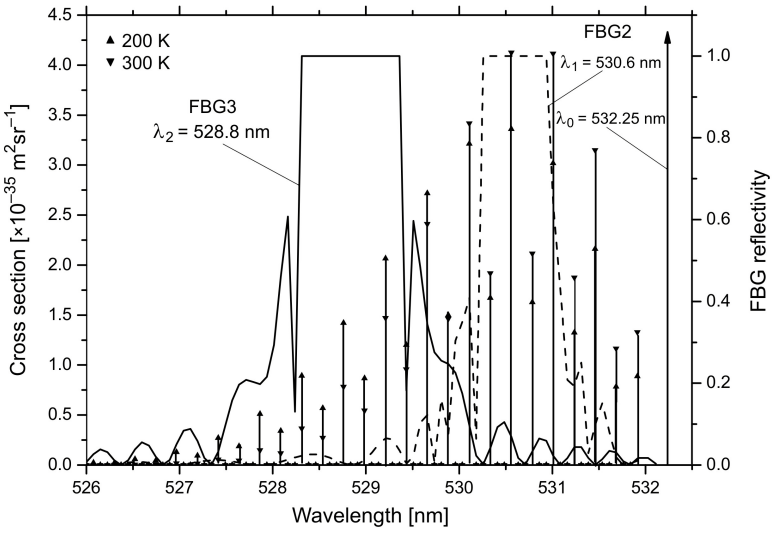

Fig. 2. Intensity of rotational Raman scattering spectra and reflectivity of FBGs.

The atmospheric temperature profile can be retrieved by analyzing the ratio of two PRR signals $R(T, z)$ as follows [10]

$$R(T, z) = \frac{n_1(T, z)}{n_2(T, z)} \approx \exp\left\{-\left[\frac{A}{T^2(z)} + \frac{B}{T(z)} + C\right]\right\} \tag{1}$$

where n_1 and n_2 are the photon number of PRR signals detected by PMT2 and PMT3, respectively, z is the height, $T(z)$ is the atmospheric temperature at height z, A, B and C are the calibration constants which can be derived by comparing the temperature data of the lidar with the data taken simultaneously with other standard instruments such as a radiosonde.

4. Design of the spectroscopic characteristic of the FBG

The reflectivity of FBG can be given by [12]

$$R(\lambda, n_{eff}, L, \delta n_{eff}) = \frac{\left(2\frac{\pi\delta n_{eff}}{\lambda}\right)^2 \sinh(\gamma(\Delta\nu, n_{eff}, \delta n_{eff})L)^2}{\delta(\lambda, n_{eff})^2 \sinh(\gamma(\lambda, n_{eff}, \delta n_{eff})L)^2 + \gamma(\lambda, n_{eff}, \delta n_{eff})^2 + \cosh(\gamma(\lambda, n_{eff}, \delta n_{eff})L)^2} \tag{2}$$

The transmission of FBG can be given by

$$T(\lambda, n_{eff}, L, \delta n_{eff}) = \frac{\gamma(\lambda, n_{eff}, \delta n_{eff}))^2}{\delta(\lambda, n_{eff})^2 \sinh(\gamma(\lambda, n_{eff}, \delta n_{eff})L)^2 + \gamma(\lambda, n_{eff}, \delta n_{eff})^2 + \cosh(\gamma(\lambda, n_{eff}, \delta n_{eff})L)^2} \tag{3}$$

where

$$\beta(\lambda, n_{eff}) = 2\pi\frac{n_{eff}}{\lambda}$$

$$\gamma(\lambda, n_{eff}, \delta n_{eff}) = \sqrt{\left(2\frac{\pi\delta n_{eff}}{\lambda}\right)^2 - \left(\beta(\Delta\nu, n_{eff}) - \frac{\pi}{\Lambda}\right)^2}$$

and n_{eff}, Λ, L, λ, δn_{eff} are effective refractive index, refractive index period, length, wavelength, effective refractive index modulation of the FBG, respectively.

The design of the spectroscopic characteristic of the FBGs is taken based on the system parameters shown in Table. Figures 3**a** and 3**b** show the spectral transmission and reflectivity of three FBGs,(FBG 1–FBG 3).

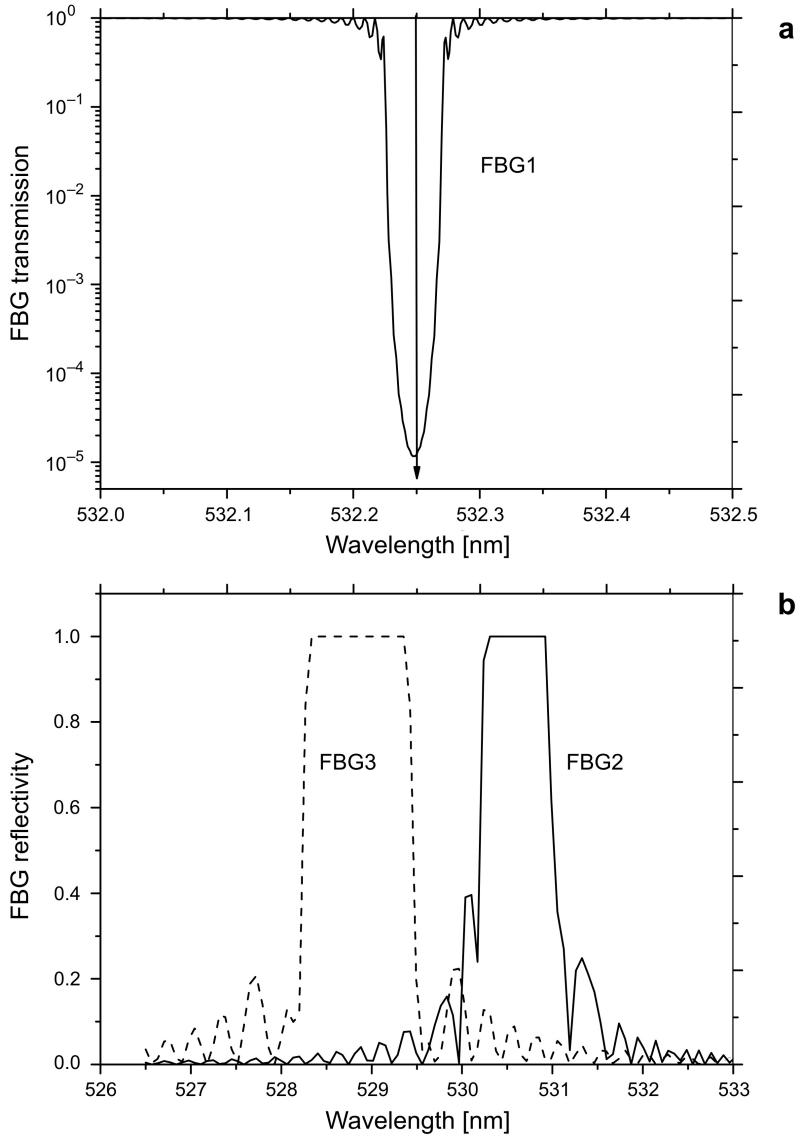

Fig. 3. Transmission of the FBG1 (**a**), reflectivity of the FBG2 and FBG3 (**b**).

Figure 3**a** shows the transmission of the FBG1. The FBG1 reflects the major portion elastic signal at λ_0 and lets the PRR signal transmit. Considering the spectrum range of Rayleigh scattering is 3 GHz, the bandwidth of full width at half-maximum (FWHM) of FBG1 is $\Delta\lambda_{FWHM0} = 0.029$ nm. Because the FBG1 reflects mainly the Mie and Rayleigh scattering signal and lets PRR signal transmit nearly entirely, the reflectivity and transmission located at wavelength of the elastic signal λ_0 are $R_0(\lambda_0) = 0.999$, $T_0(\lambda_0) = 1.211 \times 10^{-5}$, respectively. Although a few residual Mie and Rayleigh scattering signals

leak too, the rejection rate of the FBG1 for the elastic signal is up to 5 orders of magnitude.

Figure 3**b** shows the reflectivity of the FBG2 and FBG3 at central wavelength of λ_1 and λ_2. Because those two FBGs separate mainly the PRR signal which is used for temperature retrieval from the lidar return, and ensure enough signal intensity for retrieval, they have a FWHM bandwidth of 0.330 nm and 0.528 nm, and can provide a maximum reflectivity of 0.999 and 0.999 at central wavelength of 530.6 nm and 528.8 nm, respectively. On the other hand, for blocking further residual elastic signal located at λ_0, those two FBGs also provide very low transmission at λ_0, for example, $T_1(\lambda_0) = 6.068 \times 10^{-3}$, $T_2(\lambda_0) = 5.683 \times 10^{-3}$, respectively, corresponding to the rejection rate greater than 2 orders of magnitude for elastic signal. Therefore, the total rejection rate of the spectroscope system for the elastic signal is up to 7 orders of magnitude for two PRRSs.

5. Couple efficiency between telescope and single mode fiber

Because the largest light loss in the design of PRRL may be from the coupling of the telescope and the fiber, the coupling efficiency between the telescope and the fiber must be taken into consideration carefully. Generally, the multi-mode fiber is usually employed in practical lidar system to achieve relatively high coupling efficiency because of its large core diameter. However, the spectral characteristic of Bragg grating formed with multi-mode fibers show multiple reflection peaks or multiple transmission dips, which limit it to be used as a spectroscopic filter of the lidar. Therefore, the single fiber Bragg gratings are only chosen in our lidar system.

STENHOLM and DEYOUNG [11] of the NASA Langley Research Center have developed a space-based water vapor differential absorption lidar (DIAL) system. In their lidar system the single mode fiber was employed to couple the return signal from the telescope, and the fiber Bragg grating filters also were used to act as the spectroscope, they obtained the coupling efficiency between the telescope and the SMF 1.4 percent in theory and only 0.46 percent in experiment.

In our PRRL system, the laser beam expander is 10×, corresponding laser beam divergence angle θ is 0.05 mrad; the focal length f and diameter D of receiving telescope are 1000 mm and 500 mm, respectively. Also core diameter of a single mode fiber is 10 μm, and numerical aperture NA is 0.24, which is determined by $f/D = 0.5[(1/\mathrm{NA})^2 - 1]^{1/2}$ [13]. Therefore, when the lidar return is coupled into a fiber whose end face is placed at the infinity focal plane of receiving telescope, a blur disk image with diameter of 50 μm determined by $d_i = f\theta$, is formed at the infinity focal plane.

GAO *et al*. [14] have determined the relationship between coupling efficiency and deviation *s*, which is a displacement between center of blur disk image and that of fiber core for Gaussian laser beam. Figure 4 shows the coupling efficiency of SMF ver-

sus deviation *s*. It is clearly shown that the maximum coupling efficiency is 5% when *s* is 0, and coupling efficiency is 3.7 percent when *s* is 20 μm. Therefore, the low efficiency is not an intrinsic problem and it can be improved by optimizing the lidar performance in practice.

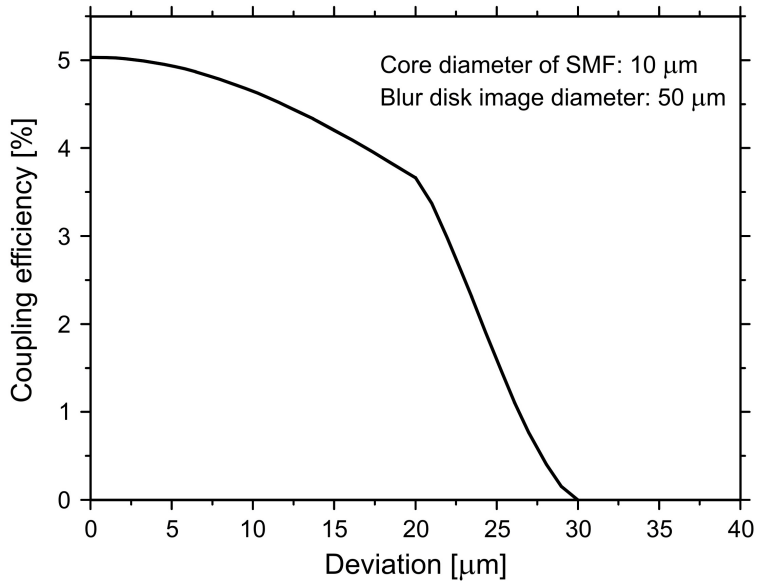

Fig. 4. Coupling efficiency of the telescope and the SMF.

6. Numerical simulation

A numerical calculation is simulated by using the configuration parameters of PRRL shown in the table and a special atmospheric model, into which a standard model and an actual Mie scattering profile obtained from observation, had been incorporated. Figure 6**b** shows the atmosphere model given in the form of backscattering ratio. Also, it should be pointed out that the numerical calculation is carried out under condition when the geometry overlap factor is equal 1.

Figure 5 shows the intensities of the lidar return and solar background passing through the FBGs with the observation time of 20 min, 24000 shots averages, range resolution of 45 m and solar radiance of 3×10^8 W·m^{-2}·sr^{-1}·nm^{-1}. Because the lidar receiver is designed to have a small field of view (FOV) of 0.01 mrad, and FBG2 and FBG 3 are designed to have very narrow bandwidth, so the solar can be reduced dramatically. According to solar radiance and system parameters of the table, the intensities of solar background at central wavelength of λ_1 and λ_2 are 9.151×10^{-13} W, 1.464×10^{-12} W, respectively. Figure 5 shows the intensities of solar background at central wavelength of λ_2.

Table. System parameters of PRRL.

Injection-seeded Nd:YAG laser	Laser wavelength [nm]	532.25
	Laser energy per Pulse [mJ]	300
	Pulse repetition rate [Hz]	20
Receiving Telescope	Diameter [mm]	500
	Field of view [mrad]	0.01
	Core diameter of fiber [μm]	10
	Numerical aperture of fiber	0.24
Spectroscope based on FBGs	Fiber Bragg grating filter	FBG1, FBG2, FBG3
	Bragg wavelengths [nm]	532.25, 530.6, 528.8
	Effective refractive index	1.462, 1.458, 1.453
	Length [mm]	9, 5, 1
	Effective refractive index modulation	6×10^{-5}, 1×10^{-3}, 1.5×10^{-3}
	Full width at half-maximum(FWHM) [nm]	0.029, 0.33, 0.528
Detector system	Detection quantum efficiency	0.26

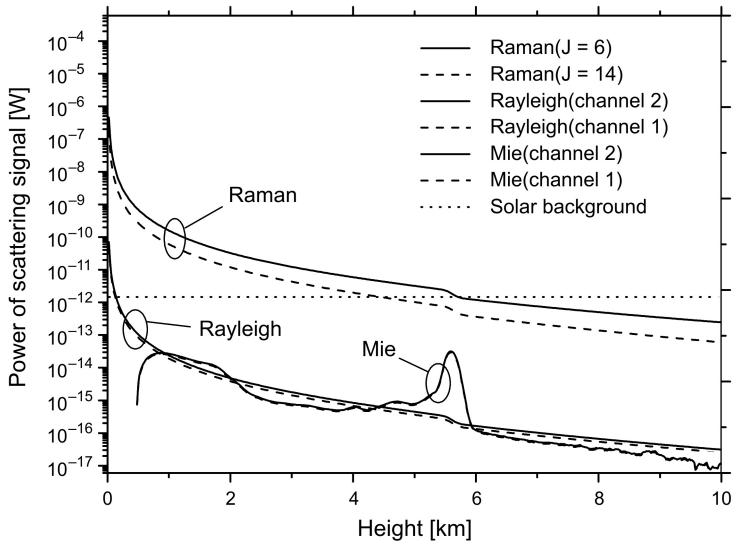

Fig. 5. Intensity distributions of lidar return and solar background versus height calculated with the parameters shown above.

Using the standard atmosphere model and the simulated PRR signal, the calibration parameters of system *A*, *B* and *C* can be obtained. The left-hand side of Fig. 6 shows the temperature profiles retrieved from two simulated PRR signals based on the atmospheric model. The solid curve on the left shows the standard model of atmospheric temperature profile, and the dashed curve shows the retrieved temperature profile that is derived by use of the assumption of the rejection capability of the FBGs for the elastic signal larger than 7 orders of magnitude.

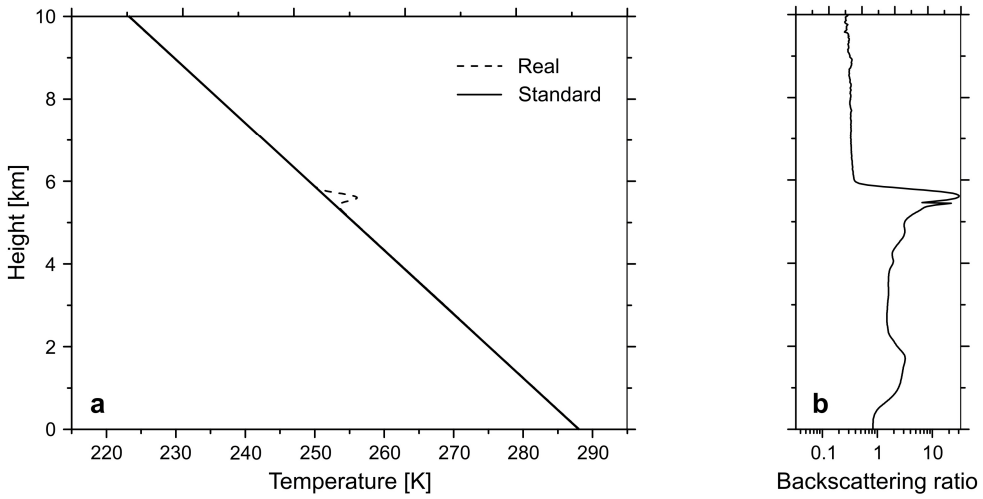

Fig. 6. Temperature profiles versus height obtained by simulation (**a**), the backscattering ratio (**b**).

It is clearly shown that the simulated temperature profile shows a good agreement with the standard temperature model at a height range of less than 5 km or larger than 7 km, in which range of the atmospheric backscattering ratio is less than 3.4. However, the maximum temperature offset was found at a height of ~5.8 km, where the backscatter ratio was ~30. The calculation clearly demonstrated that the system is able to measure the temperature profile under the atmospheric conditions of the backscattering ratio less than 3.4.

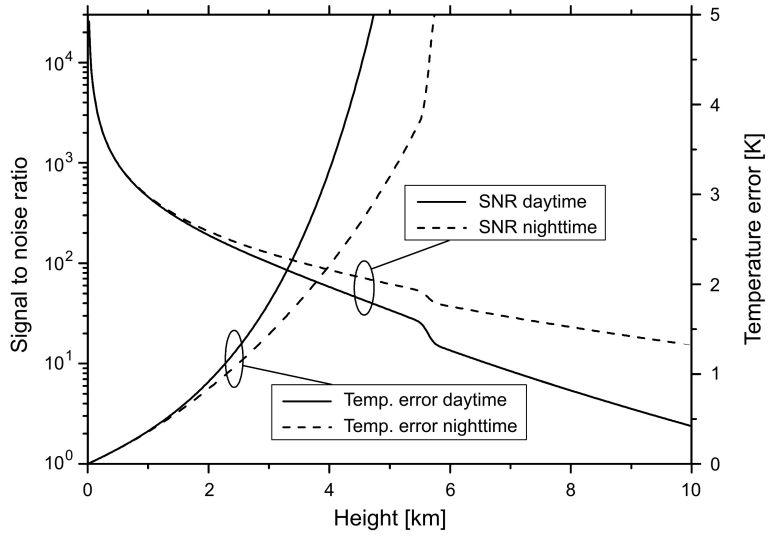

Fig. 7. The signal-to-noise ratio (SNR) and temperature error.

Because of the very narrow bandwidth of FBG2 and FBG3 and very small field of view of lidar receiver, in daytime measurement the influence of background noise which mainly arises from solar radiation decreases dramatically. Figure 7 shows the total signal-to-noise ratio (SNR) of system derived from the calculation of Fig. 5 during daytime and nighttime measurement. It is clear that the SNR, whether daytime or nighttime measurement, is approximately equal under the height of 1.8 km.

The temperature measurement sensitivity is defined as

$$S[T(z)] = \frac{1}{R(T, z)} \frac{\mathrm{d}R(T, z)}{\mathrm{d}T} \tag{4}$$

The statistical temperature measurement error that is due to SNR can be estimated from

$$e(R) = \frac{1}{\mathrm{SNR}_{\mathrm{total}}(z)\, S[T(z)]} \tag{5}$$

Figure 7 also shows the statistical temperature measurement error versus height for daytime and nighttime measurement. The results show that a statistics temperature error of less then 1 K was obtained up to a height of 2.0 km for daytime measurement, and up to a height of 2.2 km for nighttime measurement.

7. Conclusions

According to temperature dependences of intensity of PRRS of N_2 and O_2, the new type PRRL based on a FBG technique has been developed for temperature profiling in atmospheric boundary layer. The spectroscope structured with three FBGs is used to separate two PRR signals and to block the elastic signal, including the Mie- and Rayleigh-scattering signals. The rejection rate of system for elastic signal is better than 7 orders of magnitude. Because of low mass and compact of FBG, the system is relatively compact and all-fiber connection is easy to achieve. The PRRL system is simulated by using a numerical calculation, and the result shows that the PRRL based on filter characteristic of FBG is capable of measuring the atmospheric temperature vertical profiles in atmospheric boundary layer.

Regardless of the single mode fiber, which leads to decrease the receiving efficiency of lidar system, the simulation results show that the receiver and spectroscope are advantaged of daytime measurement because the small field of view of the receiver and very narrow bandwidth of FBG enhance the ability of the lidar to suppress solar background. It is suggested that the low receiving efficiency is not an intrinsic problem and it can be improved by optimizing the lidar performance in practice, such as, reducing the divergence angle of the outgoing laser beam, improving the structure design between the receiver and transmitter, enhancing the spectroscope efficiency and so on.

Acknowledgments – The work was supported by the National Natural Science Foundation of China (NSFC) (no. 40675015, 60878050) and the Universities of Science and Technology Project of Ningxia (no. 2007JY006).

References

[1] HUA D., UCHIDA M., KOBAYASHI T., *Ultraviolet Rayleigh–Mie lidar with Mie-scattering correction by Fabry–Perot etalons for temperature profiling of the troposphere*, Applied Optics **44**(7), 2005, pp. 1305–13.

[2] LIU J., HUA D., LI Y., *Rotational Raman lidar for daytime-temperature profiling of the atmospheric boundary layer*, Acta Optica Sinica **27**(5), 2007, pp. 755–59.

[3] COONEY J., *Measurement of atmospheric temperature profiles by Raman backscatter*, Journal Applied Meteorology **11**(1), 1972, pp. 108–12.

[4] HUA D., LIU J., KOBAYASHI T., *Daytime temperature profiling of planetary boundary layer with ultraviolet rotational Raman lidar*, Japanese Journal Applied Physics **46**(9A), 2007, pp. 5849–52.

[5] ARSHINOV Y.F., BOBROVNIKOV S.M., ZUEV V.E., MITEV V.M., *Atmospheric temperature measurements using a pure rotational Raman lidar*, Applied Optics **22**(19), 1983, pp. 2984–90.

[6] BEHRENDT A., NAKAMURA T., ONISHI M., BAUMGRAT R., TSUDA T., *Combined Raman lidar for the measurement of atmospheric temperature, water vapor, particle extinction coefficient, and particle backscatter coefficient*, Applied Optics **41**(36), 2002, pp. 7657–66.

[7] KIM D., CHA H., *Pure rotational Raman lidar for atmospheric temperature measurements*, Journal of the Korean Physical Society **39**(5), 2001, pp. 838–41.

[8] NEDELJKOVIC D., HAUCHECORNE A., CHANIN M., *Rotationsl raman lidar to measure the atmospheric temperature from the ground to 30 Km*, IEEE Trans. Geosci. Remote Sens. **31**(1), 1993, pp. 90–101.

[9] BALIN I., SERIKOV I., BOBROVNIKOV S., SIMEONOV V., CALPINI B., ARSHINOV Y., BERGH H.V.D., *Simultaneous measurement of atmospheric temperature, humidity, and aerosol extinction and backscatter coefficients by a combined vibrational-pure–rotational Raman lidar*, Applied Physics B. **79**(6), 2004, pp. 775–82.

[10] BEHRENDT A., REICHARDT J., *Atmospheric temperature profiling in the presence of clouds with a pure roatational Raman lidar by use of an interference-filter based polychromator*, Applied Optics **39**(9), 2000, pp. 1372–8.

[11] STENHOLM I., DEYOUNG R.J., *Ultra narrowband optical filters for water vapor differential absorption lidar (DIAL) atmospheric measurements*, NASA/TM-2001-211261, 2001, p. 20.

[12] BI W., LI L., CHEN J., LI L., *Least narrowband spectrum properties of fiber Bragg grating*, Journal of Applied Optics **28**(2), 2007, pp. 212–5 (*in Chinese*).

[13] JENNESS J.R., Jr., LYSAK D.B., Jr., PHILBRICK C.R., *Design of a lidar receiver with fiber-optic output*, Applied Optics **36**(18), 1997, pp. 4278–84.

[14] GAO F., HUA D., WU M., MAO J., ZHOU Y., *Effect of M^2 factor of laser beam for a non-coaxial lidar system*, Acta Optica Sinica **28**(9), 2008, pp. 1649–54 (*in Chinese*).

Received January 9, 2008
in revised from March 26, 2008